

Electronic Supplemental Information for:  
Regulating Aggregation of Colloidal Particles in an  
Electro-Osmotic Micropump

Zhu Zhang<sup>\*1</sup>, Joost de Graaf<sup>2</sup>, and Sanli Faez<sup>1</sup>

<sup>1</sup>Nanophotonics, Debye Institute for Nanomaterials Science, Utrecht University, Princetonplein  
1, 3584 CC Utrecht, The Netherlands

<sup>2</sup>Institute for Theoretical Physics, Center for Extreme Matter and Emergent Phenomena,  
Utrecht University, Princetonplein 5, 3584 CC Utrecht, The Netherlands.

\*E-mail: z.zhang@uu.nl

# Ionic currents

Additional data on the measured ionic currents, see Fig. 4 of the main text, for different salt concentrations. Figures S1, S2, and S3 show the ionic current passing through the channel as a function of time for salt concentrations in the top reservoir of  $C_T = 1, 2,$  and 10 mM, respectively. Figure S4 shows that ionic current passing through the channel as a function of time, after applying an DC electric potential for 10 minutes. Figure S5 shows that current passing through the channel is robust to long-term exposure to a square-wave potential.

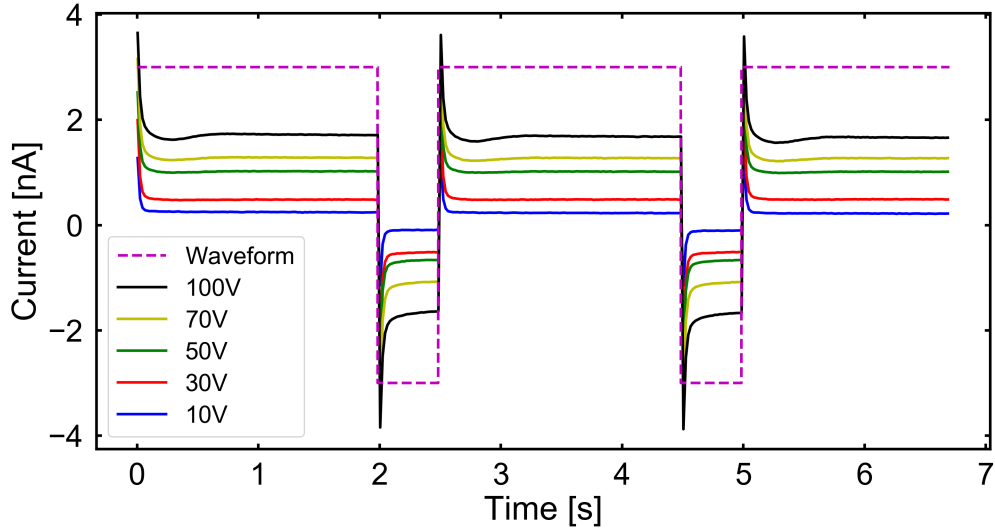


**Figure S1:** The ionic current passing through the channel as a function of time, when subjected to a square-waveform potential with period 2.5 s, duty cycle 80%, and amplitude 10 V (blue), 30 V (red), 50 V (green), 70 V (yellow), and 100 V (black). The purple dashed line indicates the shape of the applied waveform. The salt concentration in the top reservoir was  $C_T = 1$  mM, the salt concentration in the bottom reservoir was that of DI water:  $C_B \approx 0$  mM.

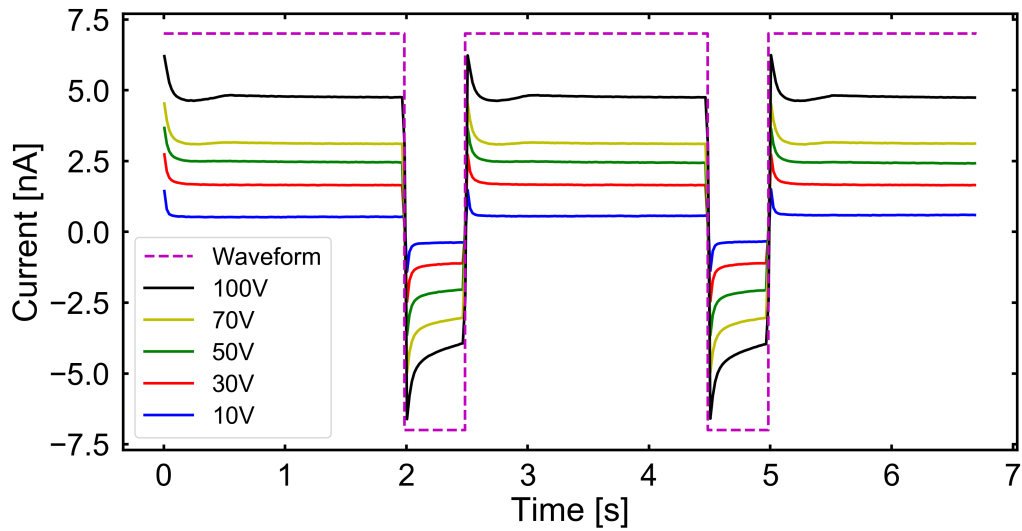


**Figure S2:** The ionic current passing through the channel as a function of time; the labeling and applied square wave are identical to Figure S1. The salt concentration in the top reservoir was  $C_T = 2$  mM, the salt concentration in the bottom reservoir was that of DI water:  $C_B \approx 0$  mM.

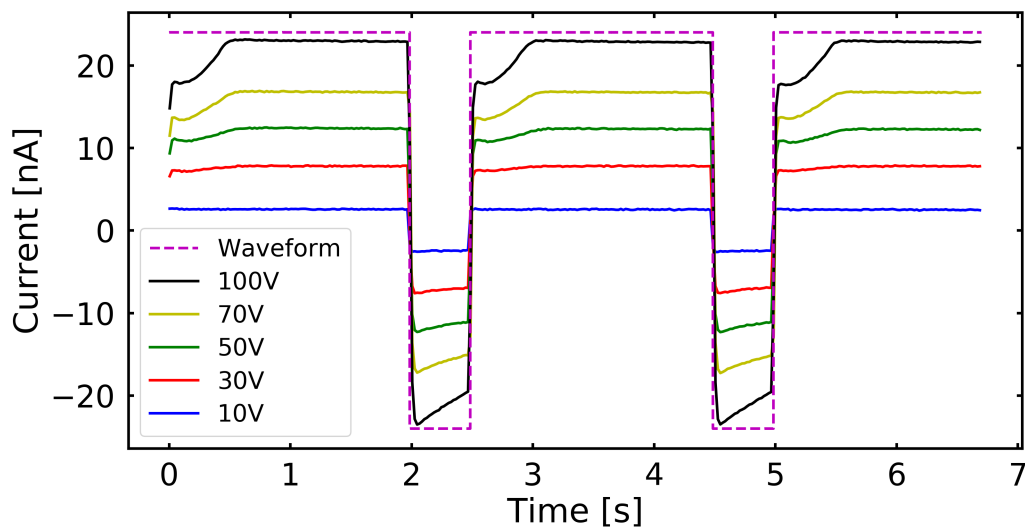


**Figure S3:** The ionic current passing through the channel as a function of time; the labeling and applied square wave are identical to Figure S1. The salt concentration in the top reservoir was  $C_T = 10$  mM, the salt concentration in the bottom reservoir was that of DI water:  $C_B \approx 0$  mM.

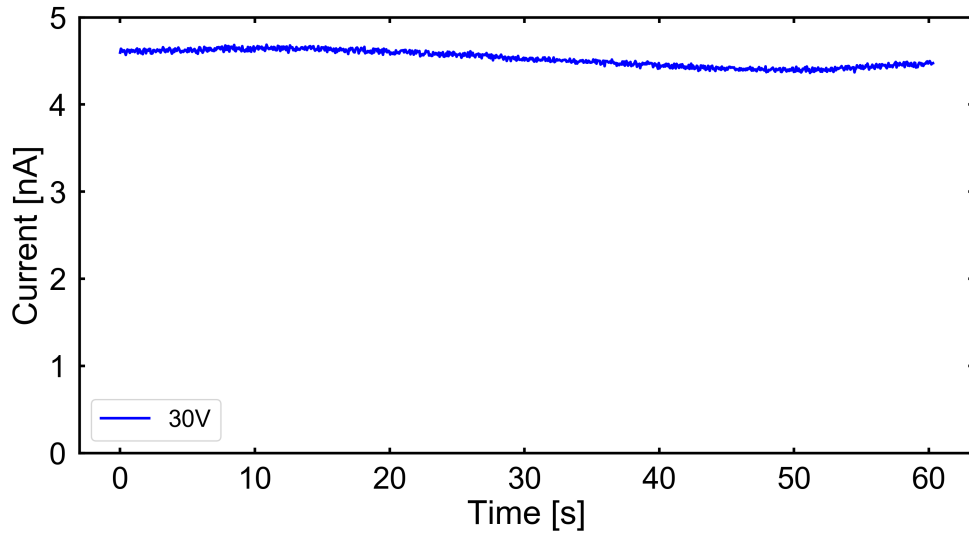


**Figure S4:** The ionic current passing through the channel as a function of time, measured after applying an DC electric potential for 10 minutes with amplitude of 30 V. The salt concentration in the top reservoir was  $C_T = 5$  mM, the salt concentration in the bottom reservoir was that of DI water:  $C_B \approx 0$  mM.

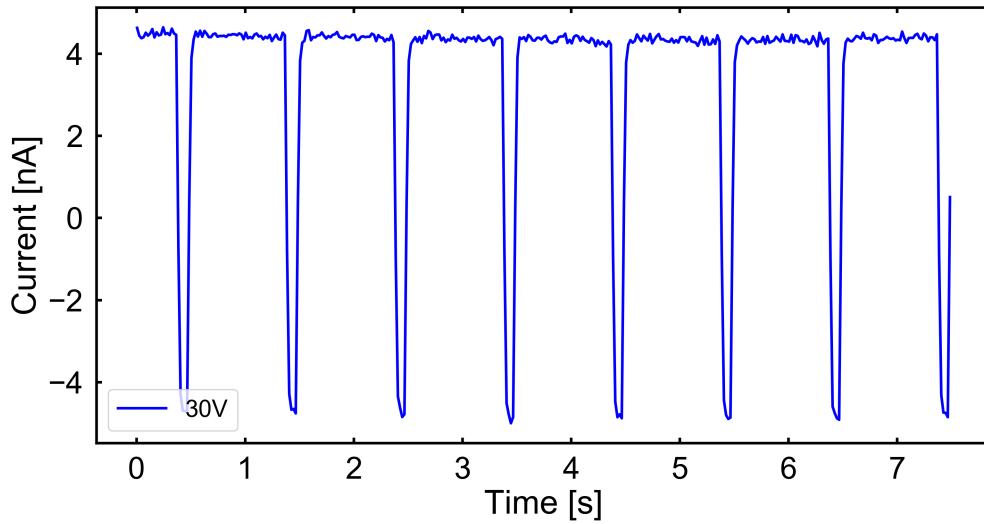


**Figure S5:** The measured ionic current passing through the channel as a function of time, measured after applying an asymmetric square-waveform electric potential for 10 minutes with period of 1 s, duty cycle of 90% and amplitude of 30 V. The salt concentration in the left reservoir was  $C_L = 5$  mM, the salt concentration in the right reservoir was that of DI water:  $C_R \approx 0$  mM.

## Clogging and Unclogging time

We quantified our AC potential's ability to clog and unclog the pore further with respect to the data presented in Fig. 3 of the main text. That is, we applied a range of signal amplitudes and T-reservoir salt concentrations. Figure S6a gives an indication of the size of the colloidal cluster that formed for a range of parameters at an imposed salt concentration of  $C_T = 5$  mM. Clearly, as the potential is increased, the intensity grows and thus the size of the cluster near the pore opening. The reversed potential proved sufficiently strong in all cases to remove the cluster.

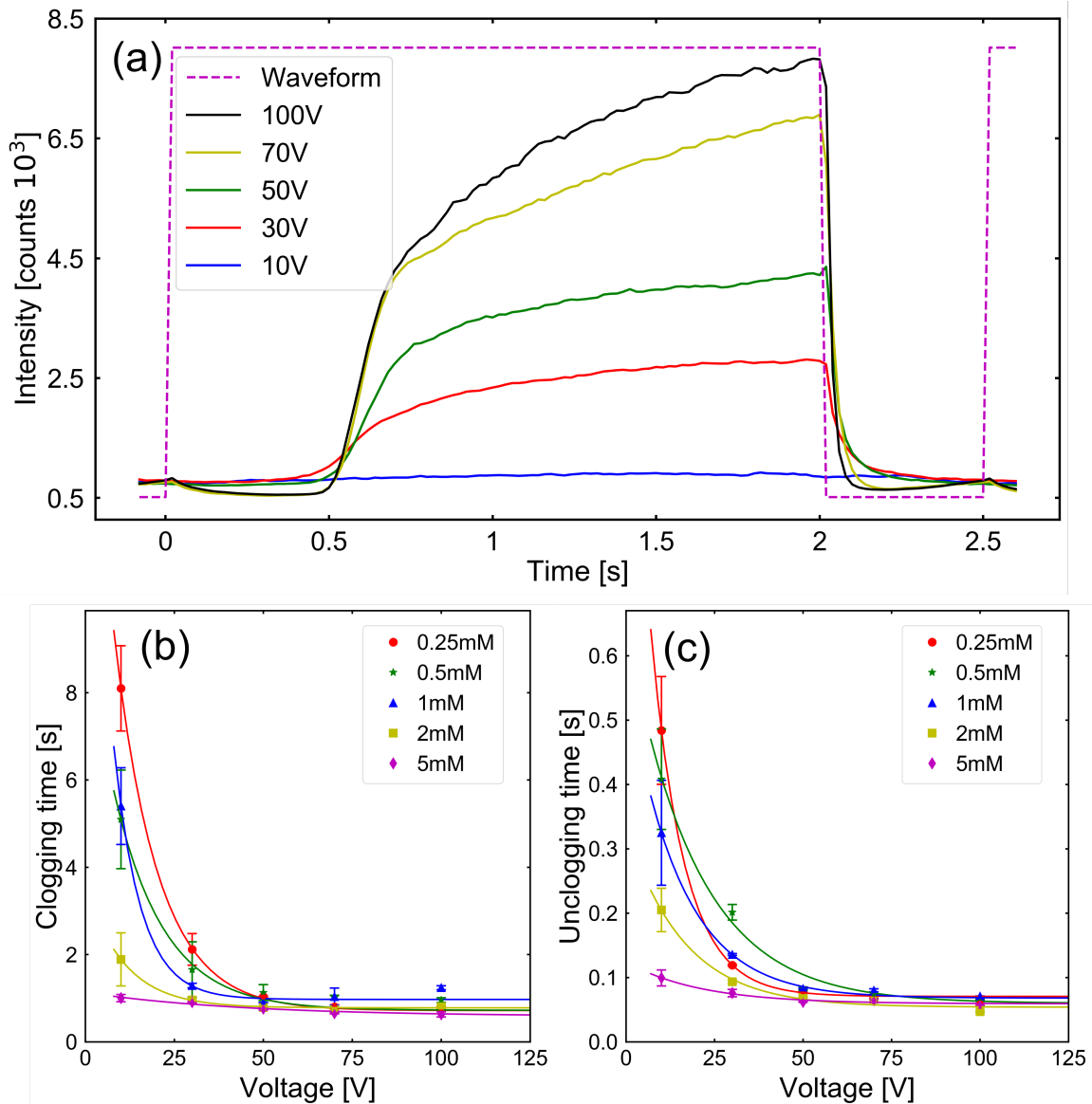


**Figure S6:** Characterizing the clogging and unclogging of the pore. (a) Colloid fluorescence intensity (in counts) as a function of time (seconds) for several values of the applied potential as indicated using colors. In all cases, the period of the square-waveform (purple dashed curve) was 2.5 s and the duty cycle was 80%. The imposed salt concentration were  $C_T = 5$  mM and  $C_B \approx 0$  mM, respectively. (b) The clogging time  $\tau_c$  (seconds) as a function of the applied potential amplitude (volts) for different values of  $C_T$ . (c) The corresponding unclogging time  $\tau_u$  also in seconds. The symbols indicate the result of our calculation, the error bars provide the standard error, and curves serve as guides to the eyes.

We divided each intensity curve in the Figure S6a, as well as the associated curves for the different salt concentrations that we employed, up into three time intervals in order to extract the relevant time scales. The first starts when the potential reverses back to positive and continues up to the point of a sharp increase in the intensity signal ( $0 - \approx 0.5$  s), we refer to the end-point as the “onset time”  $\tau_o$ . The second corresponds to the intensity increase that persists until the potential is reversed ( $\approx 0.5 - 2.0$  s). We fitted an exponential function to the intensity curve in this interval to obtain a “aggregation time”  $\tau_a$ . The third corresponds to the time over which we reversed the potential ( $2.0 - 2.5$  s). Here, we also fitted an exponential function to the intensity curve to obtain an “unclogging time”  $\tau_u$ . The total time for clogging — the “clogging time” — is now given by  $\tau_c = \tau_o + \tau_a$ . Figures S6b and S6c depict these respective times for a range salinities and applied potential. The clogging time thresholds around 1.0 s for sufficiently high applied potentials (50 V), whilst the unclogging time is systematically about a factor 10 smaller, thresholding at around 0.1 s. Below  $\approx 50$  V, both times increase with decreasing voltage.

# Numerical Modeling

In this section, we provide additional details for the numerical modeling described in the main text. In all cases, we ensured that the mesh refinement and domain size were sufficient to obtain accurate results, both in terms of convergence and finite-size effects, following the procedures outlined in Refs. 1, 2. Unlike in those references, we do not explicitly resolve the double layer, due to the much larger separation of length scales in our system. Figure S7 shows details of the meshing near the tip of the pore, where it is most refined. Note that we have used a rounding of the corners with diameter 500 nm to smooth out the transition. The inside of the pore is described using a “mapped” mesh with increasing refinement toward the wall of the channel. The full domain size is not shown in Fig. S7, but the mesh is sufficiently dense over this area.

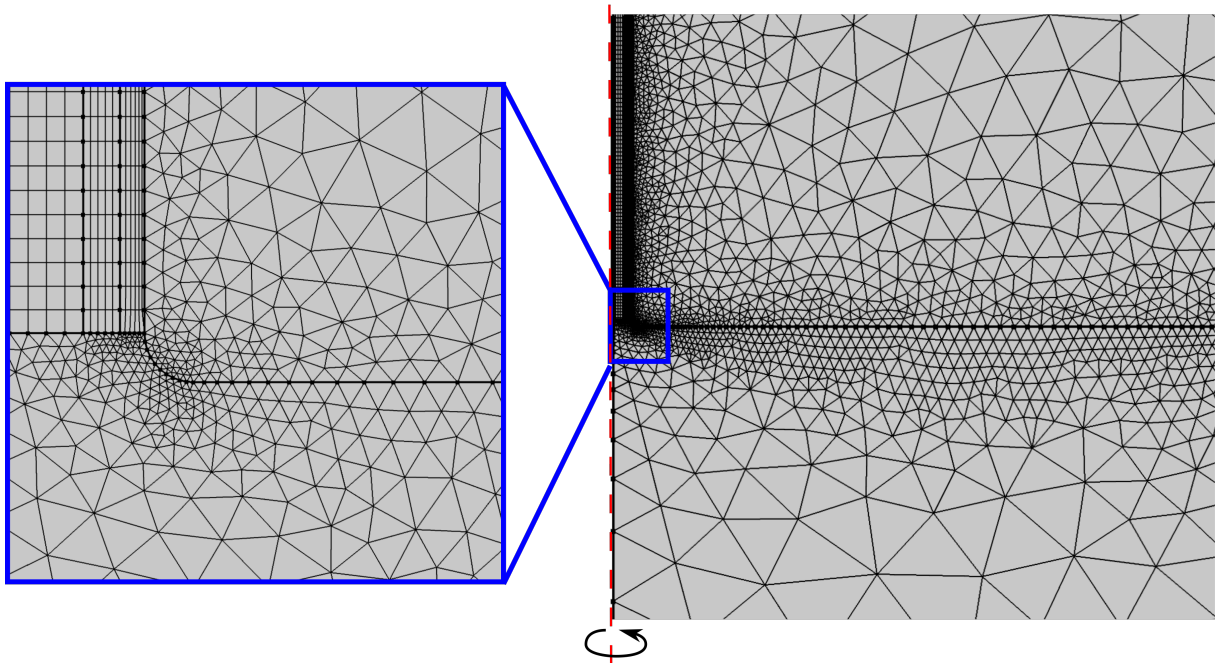
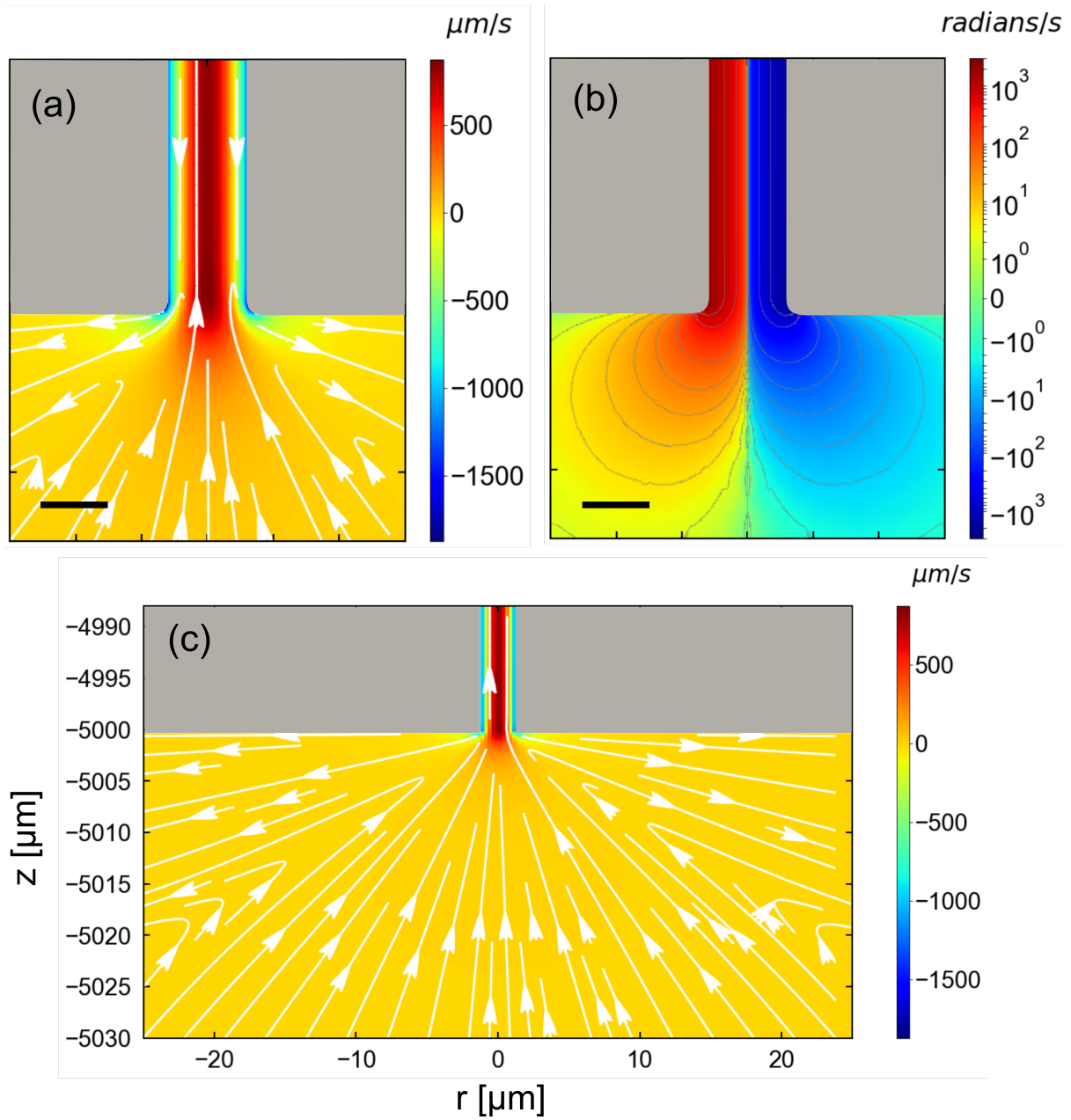


**Figure S7:** Details of the mesh used in the discretization of the channel geometry. The left-hand side shows a zoom-in of the region directly at the bottom opening. The dashed red line indicates the rotational symmetry axis for this axisymmetric problem.

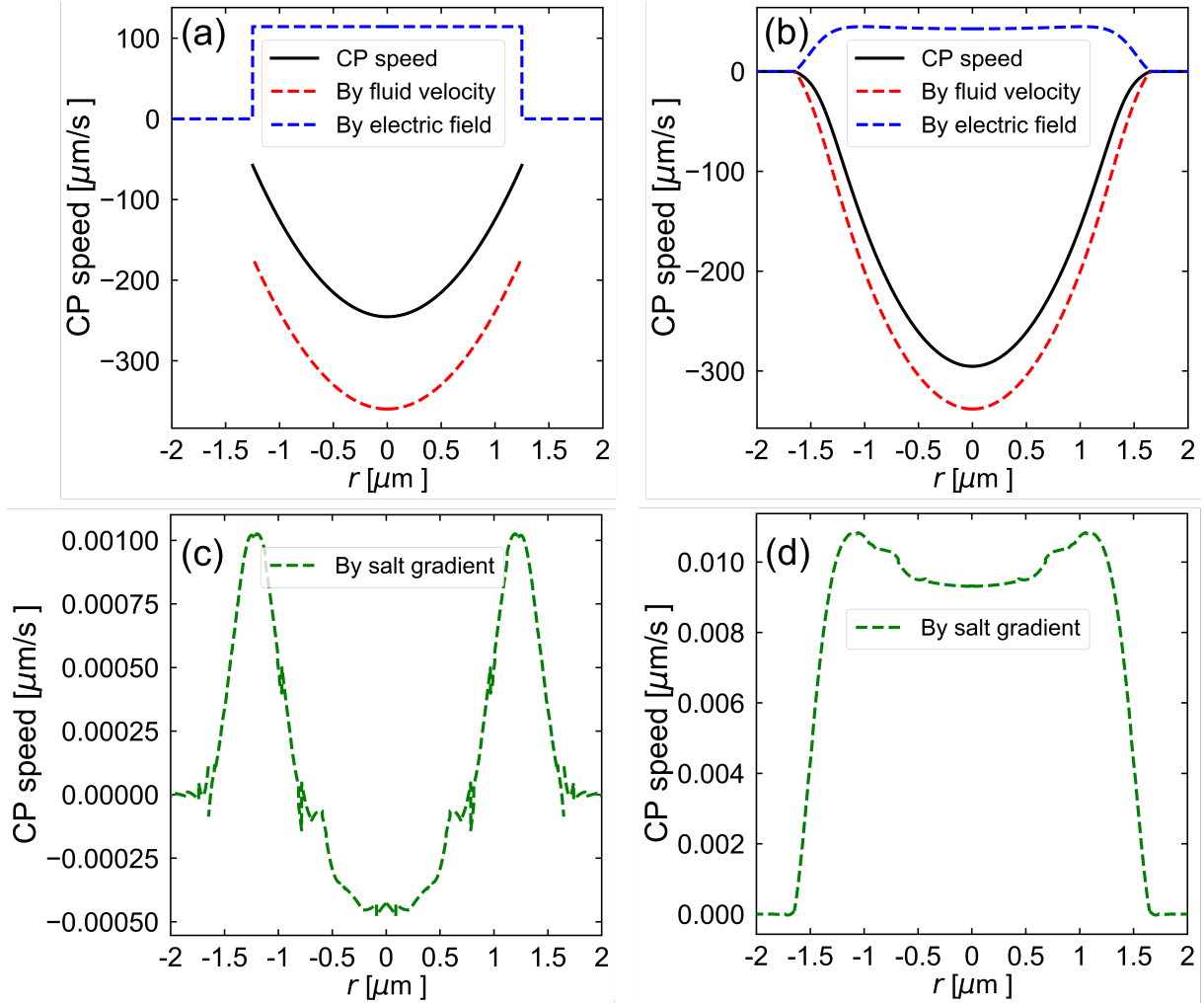
Figure S8 shows that vortices develop around the opening of the pore. This is most clearly evidenced by the vorticity parameter. As the zoom-out in Fig. S8c shows, the core of the vortex is located very far from the pore mouth.

Figure S9 shows the evolution of the CP speed along the pore, complementing the representation in Fig. 7a of the main text. Clearly, the competitive effect of the advective and electro-phoretic component give rise to sign changes in the total NP velocity only at the bottom pore opening (Fig. 7a).

Lastly, Fig. S10 shows the behavior of the hydrostatic pressure along the pore as obtained from our numerical modeling. It is clear that there is an adverse pressure gradient, which causes the flow to reverse.



**Figure S8:** Fluid velocity field (a) and vorticity field (b) at the bottom opening of the pore. (c) a zoom-out view of the fluid velocity. (a,c) White curves with arrows indicate the flow lines to the fluid velocity, the color scale provides the speed along the axial direction. (c) The color scale shows the signed value of the vorticity vector, while the grey curves provide equi-vorticity surfaces. In all figures the pore is indicated in grey. Scale bars are  $2 \mu\text{m}$



**Figure S9:** Characterization of the colloid velocity around (a,c) the middle of the pore and (b,d) the top pore opening. The parameters used are  $V_{\text{app}} = 100$  V,  $C_T = 7.5$  mM, and  $C_B = 0.5$  mM. The CP speed along the channel (black curve) — plotted here as a function of  $r$  which measures distance across the channel — is broken down into its constituents. The red dashed curves show the advective contribution, the blue dashed curves the electro-phoretic component, and green curves in (c) and (d) show the much smaller effect of ionic-diffusio-phoresis.

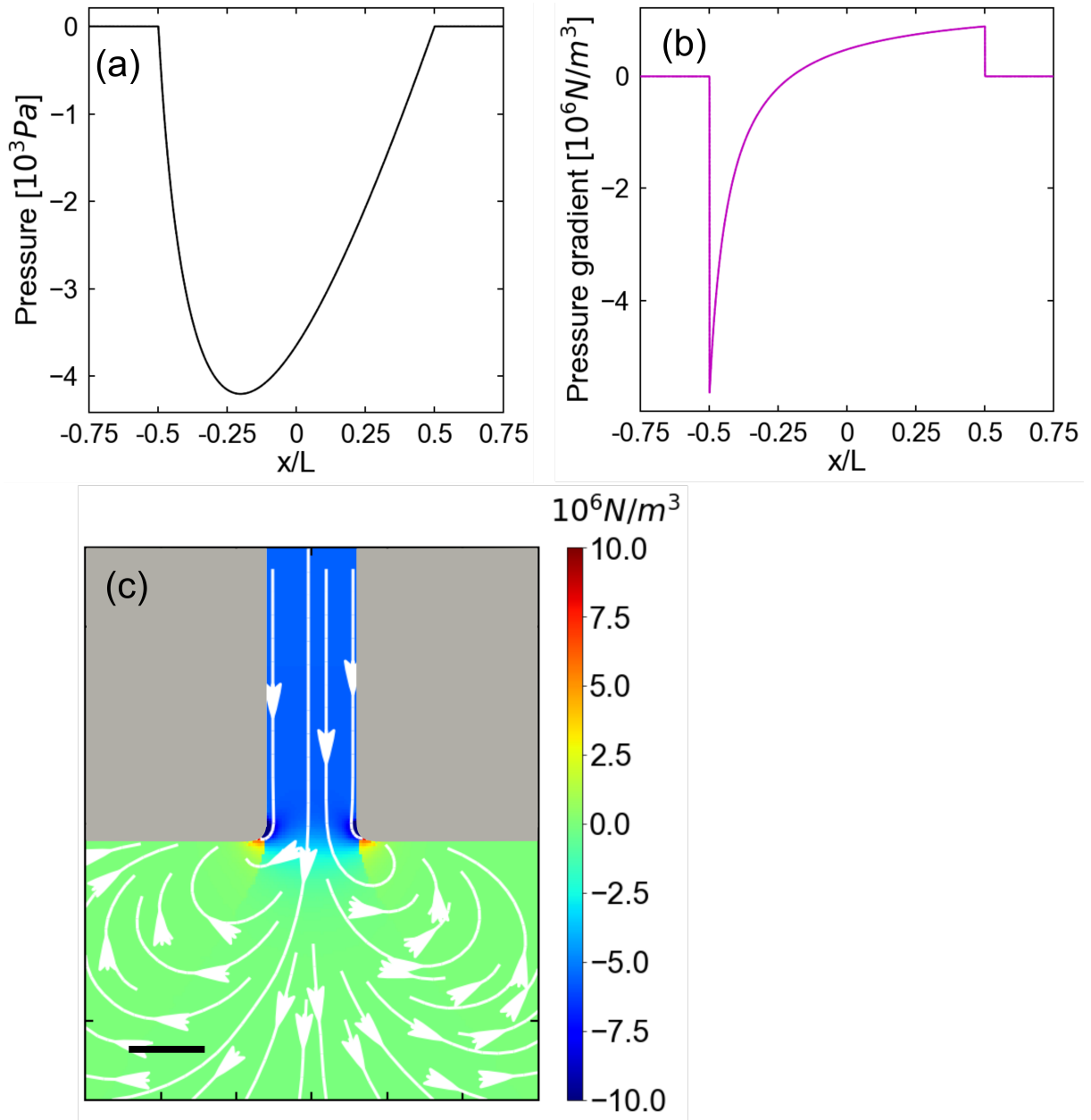


**Figure S10:** Hydrostatic pressure (a) and pressure gradient (b) along the channel measured by  $x$  (normalized by the channel length  $L$ ). The parameters used are  $V_{\text{app}} = 100 \text{ V}$ ,  $C_{\text{T}} = 7.5 \text{ mM}$ ,  $C_{\text{B}} = 0.5 \text{ mM}$ . (c) Pressure gradient field at the bottom opening of the channel. The white curves with arrows show flow lines to the vector field and the colors indicate the value of the pressure gradient in the axial direction. The scale bar is  $2 \mu\text{m}$ .

## Supplementary Movies

We have added three movies that respectively visually clarify the accumulation of nanoparticles and clogging under a DC electric field, see also Fig. 2 of the main text; the unclogging of the pore upon reversing the potential, see also Fig. 3 of the main text; and the transport of nanoparticles through the channel under the application of a square-waveform potential with appropriately tuned duty cycle, see also Fig. 5 of the main text.

**Supplementary Movie 1** showing the intensity of NPs around the bottom opening of the channel with uni-direction applied potential of 100 V (Cathode T and Anode B). The salt concentration in the upper reservoir was  $C_T = 5$  mM, the salt concentration in the bottom reservoir was  $C_B \approx 0$  mM (DI water).

**Supplementary Movie 2** showing the intensity of NPs around the bottom opening of the channel with an applied asymmetric square-waveform potential with a period of 2.5 s, a duty cycle of 80%, and an amplitude of 30 V (playing speed is slowed down  $5 \times$  to show the rapid process of NPs clogging and unclogging). The system was otherwise the same as for Supplementary Movie 1.

**Supplementary Movie 3** showing tracks of nanoparticles inside of the channel (red dashed outline), as indicated by streaks of high intensity (gray) against a black background. The tracks were observed after applying an asymmetric square-waveform electric potential for 10 minutes with period of 1 s, duty cycle of 90%, and amplitude of 30 V. The salt concentration in the left and right reservoir was  $C_L = 5$  mM and  $C_R \approx 0$  mM (DI water) respectively.

## References

1. Rempfer G, Ehrhardt S, Holm C, and de Graaf J. Nanoparticle Translocation through Conical Nanopores: A Finite Element Study of Electrokinetic Transport. *Macromolecular Theory and Simulations* 2017;26:1600051.
2. Rempfer G, Ehrhardt S, Laohakunakorn N, et al. Selective Trapping of DNA Using Glass Microcapillaries. *Langmuir* 2016;32:8525–32.